Solar Energy Materials & Solar Cells 146 (2016) 121–128

Contents lists available at ScienceDirect

Solar Energy Materials & Solar Cells

journal homepage: www.elsevier.com/locate/solmat

Arrays of CZTS sensitized ZnO/ZnS and ZnO/ZnSe core/shell nanorods for liquid junction nanowire solar cells

Muhammad Aftab Akram [a,*], Sofia Javed [a], Mohammad Islam [b], Mohammad Mujahid [a], Amna Safdar [a]

[a] School of Chemical and Materials Engineering (SCME), National University of Sciences and Technology, Sector H-12, Islamabad 44000, Pakistan
[b] Center of Excellence for Research in Engineering Materials (CEREM), Advanced Manufacturing Institute, King Saud University, P.O. Box 800, Riyadh 11421, Saudi Arabia

ARTICLE INFO

Article history:
Received 22 April 2015
Received in revised form
17 November 2015
Accepted 22 November 2015
Available online 11 December 2015

Keywords:
CZTS
ZnO
Aligned nanorods
Core/shell structure
ZnS
ZnSe
Liquid junction solar cells

ABSTRACT

Copper–zinc–tin–sulfide (Cu_2ZnSnS_4 or CZTS) is an important p-type semiconductor material for solar cell applications. A unique architecture for liquid junction solar cell made of ZnO/Al:ZnO/ZnS or ZnSe/CZTS core/shell vertically aligned nanorods array is reported. Over fluorine-doped tin oxide (FTO) coated glass, vertically aligned Al-doped zinc oxide nanorods (VANR) were grown over ZnO seed layer. It was followed by surface transformation of ZnO nanorods to ZnS or ZnSe through solubility constant (K_{sp}) difference induced anion exchange in a S^{2-} or Se^{2-} solution to produce ZnO/ZnS and ZnO/ZnSe core–shell (CS) structures. Separately, CZTS nanoparticles were synthesized from high temperature arrested precipitation and subsequently used for sensitization of ZnO/ZnS CS-VANR nanostructures. Cu_2S and polysulfide were employed as counter-electrode and electrolyte respectively for fabrication of liquid junction solar cells. FE-SEM, HRTEM, X-ray diffraction and Raman spectroscopy techniques were employed for microstructural, morphological and compositional characterization of different component materials. The *J–V* measurements of the solar cell correspond to a several fold higher power conversion efficiency than similar device with thin film multilayer planar configuration involving same amount of materials. The aligned core/shell nanorods configuration offers an increase in the interfacial area by several folds, shorter pathway for charge transport and efficient photon absorption.

1. Introduction

Chalcogenide solar cells based on $Cu(In_{1-x}Ga_x)Se_2$ (CIGS) or CdTe have crossed the bench mark of 20% power conversion efficiency [1–3], resulting in widespread commercialization of these technologies. However, to meet the ever-growing energy needs of the world, issues related to scarcity and cost of precursors: In, Ga and Te cast doubts over long-term sustainability of these technologies. It is estimated that if all the In resources in the world would be used in fabricating commercial photovoltaic modules, it will account for only 70 GW of power generation [4,5]. The toxicity of Cd is also another hindrance in the pursuit of CdTe based thin film solar cells [6,7].

As a replacement for CIGS based compounds, exploratory research for alternative compositions involving environment-friendly, earth-abundant and inexpensive precursor elements has led to the development of Cu_2ZnSnS_4 (CZTS) p-type absorber semiconductor material. CZTS has high light absorption coefficient of the order $> 10^4\ cm^{-1}$ [8,9], and direct band gap energy value of ~ 1.5 eV [10,11]. The highest values of power conversion efficiency (PCE) reported for CZTS and CZTSe based solar cells are 8.4 [12] and 12.6% [13], respectively. Despite a high efficiency and other advantages associated with vacuum processing, drawbacks including high production cost of vacuum equipment, elevated synthesis temperatures, use of toxic gases (H_2Se or Se) and material waste [14–16], research focus has shifted to devise facile, solution based processing routes for CZTS nanocrystals and films. One of the approaches to overcome these issues involves using colloidal nanoinks of CZTS for subsequent absorber layer application under ambient or less severe processing conditions [17–21]. This heterojunction configuration, however, lowers the power conversion efficiency mainly by poor p–n junction due to small grain size and high series resistance arising from large number of grain boundaries in the path of current flow.

Solar cells with enhanced efficiencies maybe fabricated through incorporation of one-dimensional (1-D) nanostructures

* Corresponding author. Tel.: +92 321 473 7036; fax: +92 51 9085 5002.
E-mail addresses: aftabakram@scme.nust.edu.pk (M. Aftab Akram), sofiajaved@scme.nust.edu.pk (S. Javed), mohammad.islam@gmail.com, miqureshi@ksu.edu.sa (M. Islam), principal@scme.nust.edu.pk (M. Mujahid), amnasafdar28@gmail.com (A. Safdar).

http://dx.doi.org/10.1016/j.solmat.2015.11.034
0927-0248/

including nanowires, nanotubes, and nanorods. These offer great potential to improve conversion efficiency by expediting photon absorption, increasing electron mobility, and enhancing electron collection efficiency in solar cells [22–24]. Nanowire morphology of I–III–VI chalcopyrite materials can offer pathways for continuous charge carrier transport without dead ends, which is an advantage over random p–n junctions. In such devices, however, the charge carriers have to move long distances, on the order of absorber and buffer layers thicknesses, to reach the counter electrodes. This problem can be overcome through application of the absorber, buffer and window layers via facile solution synthesis in the 1-D core/shell structure configuration [25]. In this case the only disadvantage would be limited light absorption capabilities due to difficulty in producing absorber shells with greater thickness values [24].

Solar cells fabrication by employing solution processing techniques for all component layers, eliminating any needs of vacuum processing, is thus an attractive research domain to reduce extensive equipment costs. Recently, results from fabrication and testing of superstrate solar cell configurations based on vertically aligned nanorod arrays of ZnO/CdS core/shell structures coated with CZTS nanoparticles have been reported [26,27]. Although CdS is the most commonly used composition as buffer layer and has been an integral part of solar cells with record conversion efficiency, its drawbacks include inability to transmit full solar spectrum due to a relatively low band gap value ($\sim$2.4 eV), greater electron affinity as compared to CZTS or CIGS, enhanced carrier recombination rate at the relatively wider band gap absorber/CdS interface and serious environmental problems associated with CdS layer [28].

Among alternative cadmium-free buffer layer compositions, zinc sulfide (ZnS) and zinc selenide (ZnSe) have been extensively explored for CIGSSe based solar cells. ZnS is a high band gap energy material (E_g 3.8 eV) with high transmittance in the visible range [29], higher quantum efficiency of the device at short wavelengths with an associated increase in the short-circuit current (J_{SC}) of the device and a large band offset between CIGS and ZnS [30]. A power conversion efficiency of 18.6% was reported for CIGS solar cell incorporating ZnS(S, O, OH) buffer layer [31], whereas ZnS has already found its use as a standard buffer layer in commercial CIGS modules [32]. When conduction band alignment is considered for buffer-absorber interface, ZnS has been found to cause current blocking owing to a high barrier formation towards CZTS, both theoretically [33] and experimentally [34], in CZTS based solar cells. The device quality is explained in terms of the buffer/absorber heterojunction interface through critical parameters namely valence band offset (VBO) and conduction band offset (CBO) values that strongly affect charge transfer across the buffer/absorber interface. It is noteworthy that CdS/CZTS heterojunction interface has a CBO of -0.30 to 0.35 eV with a negative value indicative of cliff-like behavior [35]. Due to smaller CBO values for selenides than sulfides, ZnSe is anticipated to promote better performance attributes in solar cells incorporating ZnSe buffer layer.

In this paper, we propose and present preliminary data from fabrication and testing of solar cells with superstrate configuration employing core/shell vertically-aligned nanorod arrays (CS-VANR), polysulfide electrolyte and Cu_2S counter-electrode. Using fluorine-doped tin oxide (FTO) glass substrates, vertically aligned arrays of Al:ZnO were grown with subsequent encapsulation of individual nanorods via step-by-step application of different component layers with certain functionalities using low temperature, liquid processing routes. The solar cell configuration reported in this study is anticipated to reduce the extent of charge carrier recombination through reduction in the length of charge flow path and enhancement in light absorption due to a greater number of grain boundaries in the direction of incident photons. The incorporation of mesoporous CZTS absorber layer is an addition to the benefits of the 1-D assembly and is specialty of the present report. Using ZnS and ZnSe as the buffer layers and exploiting two different buffer/absorber interfaces in the cell structure, the effect of buffer layer composition on the *J–V* characteristics of the solar cells was also investigated.

2. Experimental work

2.1. Materials

Fluorine-doped tin oxide (FTO) coated glass slides were used as substrates for this work. All the precursor chemicals and organic solvents were procured from Sigma-Aldrich and were used as-received without any further treatment.

2.2. Solar cell fabrication

Following thorough cleaning of the FTO substrates, the initial zinc oxide (ZnO) blocking layer was applied via spin coating a sol containing 200 mM zinc acetate in 20 mL methanol and 0.41 mL acetyleacetone after it was magnetically stirred at 60 °C for 2 h and aged for 24 h at room temperature. Afterwards, the samples were heat treated at 400 °C for 0.5 h. To produce aligned arrays of aluminum-doped zinc oxide (Al:ZnO) nanorods, the FTO/i-ZnO samples were then immersed into an equimolar aqueous solution (25 mM each) of zinc nitrate and hexa-methylene-tetra-amine along with an uncoated aluminum foil at 90 °C for 3 h. After cleaning, the samples were exposed to the ultraviolet (UV) radiation for $\sim$30 min in order to induce oxygen vacancies for increased electrical conductivity [36]. Subsequent layer of ZnSe or ZnS to obtain FTO/i-ZnO /Al:ZnO/buffer configuration was obtained via ion exchange method [24,37]. The samples were then washed with deionized water and absolute ethanol and finally dried with air blow.

Nanocrystals of the composition Cu_2ZnSnS_4 (CZTS) were synthesized from high temperature arrested precipitation in oleylamine. For this purpose, halides of copper, zinc and tin were dissolved in oleylamine in molar ratios of 2:1:1 and heated to 170 °C for 30 min to obtain a clear solution. Separately, another solution was prepared by adding S powder to oleylamine. Both solutions were mixed with Cu:Zn:Sn:S molar ratio of 2:1:1:4 and the resulting mixture was heated to 230 °C for 1.5 h to ensure complete chemical reaction between precursors. The solution was later cooled and further purified by pouring into cold methanol. The nanocrytals so obtained were washed several times and separated in a centrifuge followed by overnight vacuum drying at 40 °C and annealing in inert atmosphere at 500 °C for 1 h. The annealed nanoparticles were dispersed in ethanol and spin coated at 1500 rpm to obtain FTO/i-ZnO /Al:ZnO/buffer/CZTS in the form of aligned arrays of core/shell nanorods, where buffer is either ZnS or ZnSe. Eventually, the nanostructured configuration was annealed at 400 °C for 1 h under N_2 gas flow and used as photoanode in the solar cell. To make the counter-electrode, a copper strip was immersed in a polysulfide aqueous solution containing one molar S and Na_2S along with 100 mM NaOH for 5 min [38], causing Cu_2S formation at the surface. The solar cell was fabricated by joining and bonding the Cu_2S counter electrode surface with VANR array assembly with the inter-electrode spacing filled with the polysulfide electrolyte of the same composition as that used to make the Cu_2S counter-electrode from copper.

2.2.1. Device characterization and testing

Morphological studies of the Al:ZnO nanorods, CZTS nanoparticles and core/shell nanostructures were performed by scanning electron microscope (SEM), using a field-emission SEM from Philips (XL30) or thermionic emission SEM of JEOL (JSM 6490A), and transmission electron microscope (TEM) using a field-emission (TEM; Philips CM 20). For SEM examination, the values of operating voltage and working distance were maintained at 5 kV and 15 mm for XL30 and 20 kV and 10 mm respectively for JSM 6490A, whereas TEM examination was carried out at 200 kV accelerating voltage. The phase/composition analysis was done using X-ray diffraction (XRD) machine (STOE Stadi MP) in the 2θ range of 20–70° keeping 0.04° step size and 2 s dwell time. The Raman spectra were obtained from a Renishaw 2000 laser Raman Spectroscope at 514 nm excitation wavelength for Ar^+ laser.

The performance of the individual solar cells was assessed in terms of output current density versus voltage (J–V) characteristics using a potentiostat (Biologic VSP) under 1 sun illumination (100 mW/cm^2).

3. Results and discussion

The complete scheme of solar cell fabrication is depicted in Fig. 1. A thin film of intrinsic zinc oxide (i-ZnO) acts as a seed layer for subsequent growth of aligned nanorod arrays besides isolation of the conductive FTO on glass substrate. From previous studies [39], the thickness of this layer is not anticipated to exceed beyond few tens of nanometers. An array of vertically aligned ZnO nanorods (VANR) can be produced via low temperature hydrothermal method. The length and diameter of the nanorods, area density and Al-doping level can be tailored from careful selection of processing parameters [40,41]. During treatment with solution containing S^{2-} ions, the large difference in the values of solubility product constant (K_{sp}) for $Zn(OH)_2$ and ZnS, reported to be on the order of 10^{-17} and 10^{-25}, respectively [25,42], causes spontaneous transformation of ZnO to ZnS at the Al:ZnO surface, thus changing their composition to ZnO/ZnS core/shell nanorods. Arrays of ZnO/ZnSe core/shell nanocables were synthesized by immersing the ZnO nanorod arrays in the Se^{2-} source solution obtained by dissolving Se in water in the presence of reducing $NaBH_4$ at 50 °C for 5 h. The surface as well as the space between modified VANR array is filled with an ethanol based nanoink, containing separately prepared CZTS nanocrystals, that is spin coated over ZnO/buffer core/shell nanostructures. The heterojunction configuration of FTO/ZnO/Al:ZnO/ZnS/CZTS (CS-VANR-1) or FTO/ZnO/Al:ZnO/ZnSe/CZTS (CS-VANR-2) constitutes the photoanodes. The counter electrode is made of Cu_2S, and the inter-electrode space is filled with polysulfide electrolyte to complete the fabrication of an

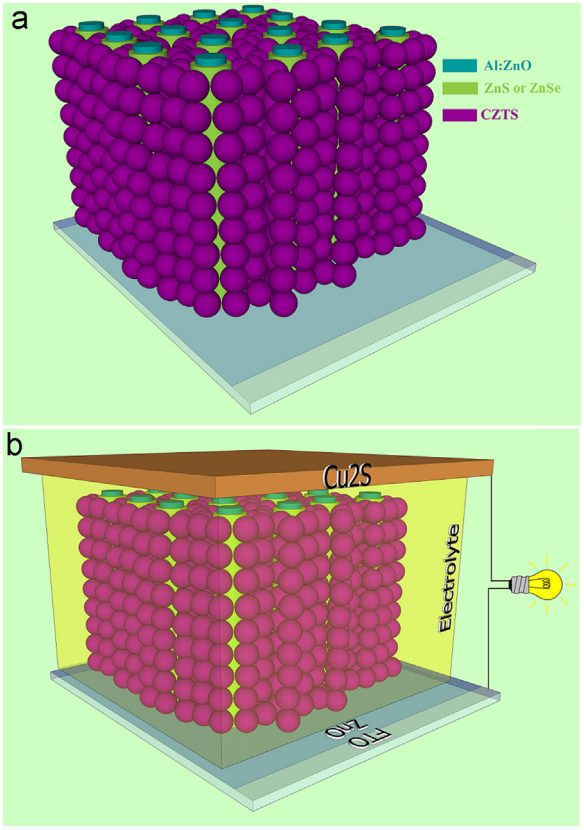

Fig. 2. (a) Three-dimensional schematic depiction of the fabricated device: (a) The photoanode showing CS-VANR coated with CZTS nanoparticles over FTO-glass substrate and (b) Individual solar cell with polysulfide electrolyte and Cu_2S counter-electrode. Components are not to scale.

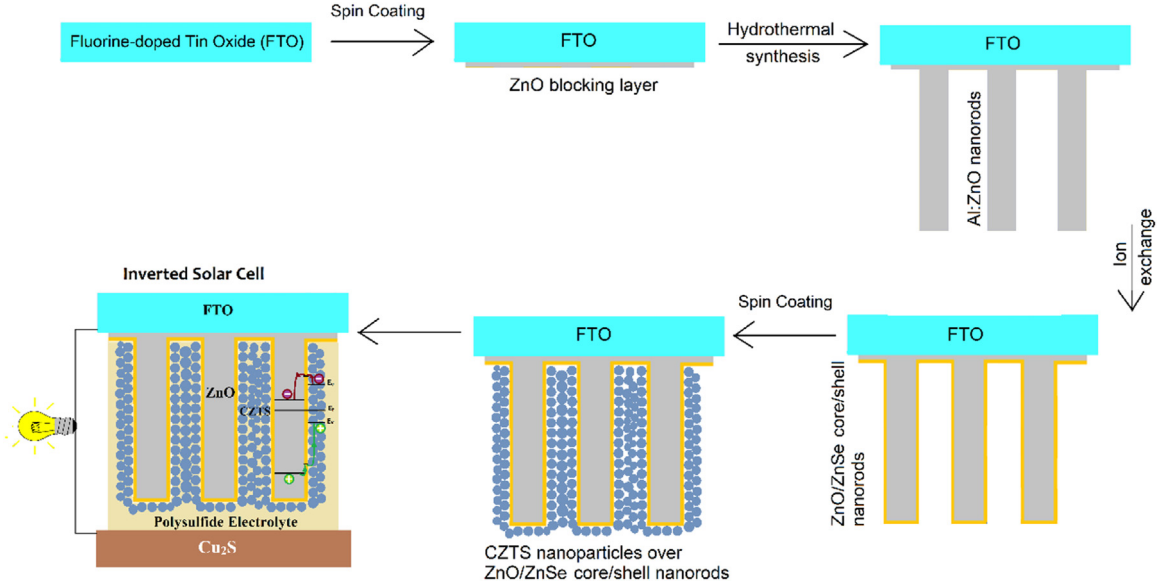

Fig. 1. Process flow diagram for fabrication of CZTS sensitized ZnO/ZnSe core/shell nanorods arrays and their subsequent application in liquid junction solar cells.

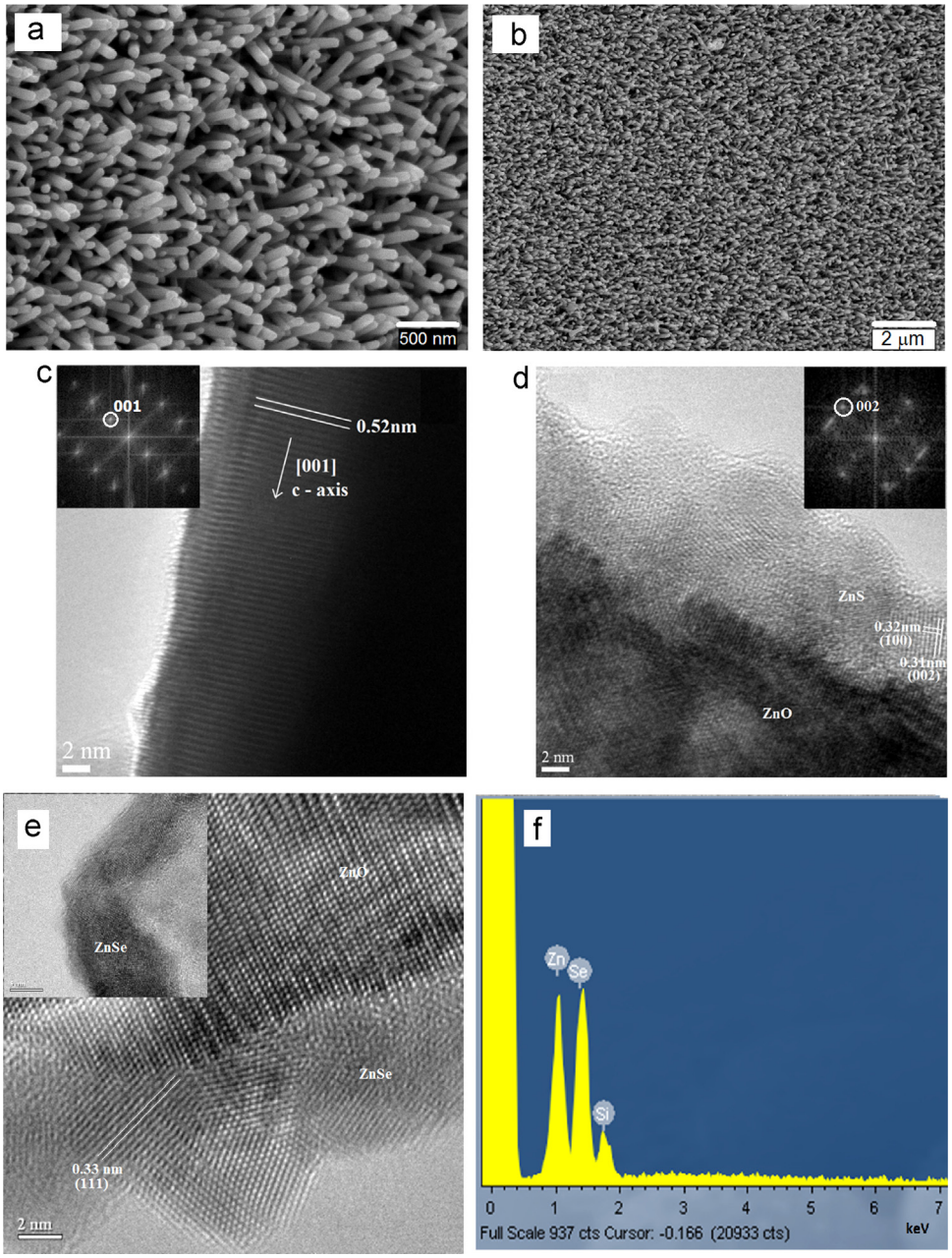

Fig. 3. FE-SEM and HR-TEM examination of (a and c) Al:ZnO nanorods and (b and d) Al:ZnO/ZnS core/shell nanostructures. The insets in b and d are FFT patterns. (e) HRTEM image of Al:ZnO/ZnSe core/shell nanorod, inset is TEM of ZnSe shell after dissolving core in acetic acid solution. (f) EDS spectrum of the ZnSe nanotubes deposited on a Si wafer, revealing a Zn/Se atomic ratio of ~1:1.

individual solar cell. The electrolyte serves as a transport medium for charge carriers generated by the CZTS nanocrystals. The experimentation scheme offers several advantages including (i) solution processing routes for all components, (ii) process adaptability for flexible substrates and (iii) a relatively low maximum processing temperature of 400 °C.

Three-dimensional schematic illustrations of the photoanode and a complete solar cell are given in Fig. 2. Spin coating of the CZTS ethanol suspension results in coverage of the CS-VANRs with CZTS nanoparticles, filling up the inter-rods spacing with subsequent formation of a mesoporus photoanode. The pores are eventually filled with the polysulfide electrolyte which acts as charge transfer medium between the two electrodes.

Electron microscopy examination of the Al:ZnO nanorods array as well as Al:ZnO/ZnS, Al:ZnO/ZnSe was performed using both FE-SEM and HR-TEM, as shown in Fig. 3. From high magnification image (Fig. 3a), the as-grown Al:ZnO nanorods appear to be well aligned almost vertical to the substrate surface with an average diameter of ~75 nm. The aspect ratio of the nanorods is thus anticipated to be in the range of 15–25, considering the fact that the average NR length is 1–2 μm. The area density of the nanorods is estimated to be approximately 62/μm^2. The HR-TEM studies, presented in Fig. 3c, indicate that the nanorods produced are highly crystalline with lattice fringes characteristic of ZnO (001) planar orientation with inter-planar spacing of 0.52 nm and preferential growth along the [001] direction. Upon Na_2S treatment, the integrity of the VANR array was not affected as evident from the large-area top-view of the sample (Fig. 3b). The transformation of ZnO to ZnS through ion exchange is evident from HRTEM microstructure where a 10-nm thick outer layer of ZnS is present (Fig. 3d). The ZnS shell so formed is polycrystalline as anion exchange process induces lattice stresses due to size difference

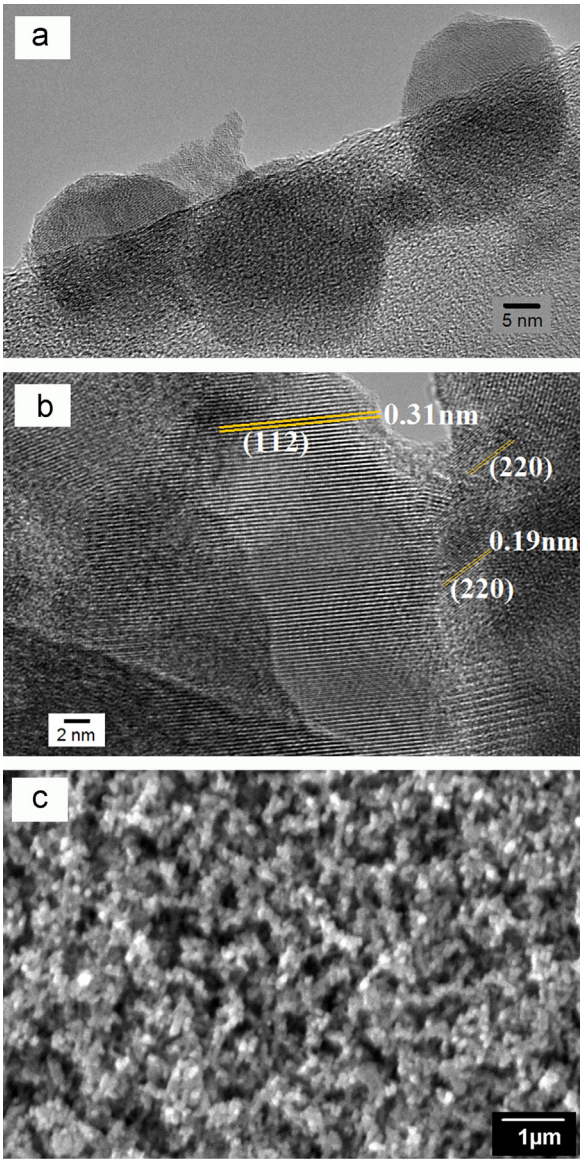

Fig. 4. (a and b) Electron microscopy results of the CZTS nanoparticles showing size, morphology and phase composition and (c) top view of the CS-VANR after spin coating with CZTS suspension and annealing.

between O^{2-} (126 pm) and S^{2-} (170 pm) ions, thus favoring polycrystalline ZnS formation from single crystal Al:ZnO. The lattice structure was indexed to be wurtzite ZnS from lattices fringes representative of (002) and (100) planes with respective interplanar spacing of 0.31 and 0.32 nm. The results demonstrate that the ion exchange treatment successfully transformed Al:ZnO nanorods into Al:ZnO/ZnS core/shell structure. Besides indexing of the diffraction fringes seen in the HRTEM microstructures, the phase structure can also be confirmed from FFT patterns obtained for the Al:ZnO core and ZnS shell of the nanorod. HRTEM image of Al:ZnO/ZnSe core/shell structure is shown in Fig. 3e. ZnSe shell is again polycrystalline as its crystal structure is cubic which is different than hexagonal structure of ZnO so it will form its own crystallites and the shell thickness is around 10 nm as revealed by TEM image of hollow ZnSe tube obtained after dissolving ZnO core in acetic acid (inset Fig. 3e). The EDS spectrum from ZnSe hollow tube is given in Fig. 3f revealing Zn/Se atomic ratio of about 1:1.

The morphology and phase composition of the CZTS nanoparticles are presented in Fig. 4. The as-produced nanoparticles are of spherical shape with an average size of ~20 nm. The

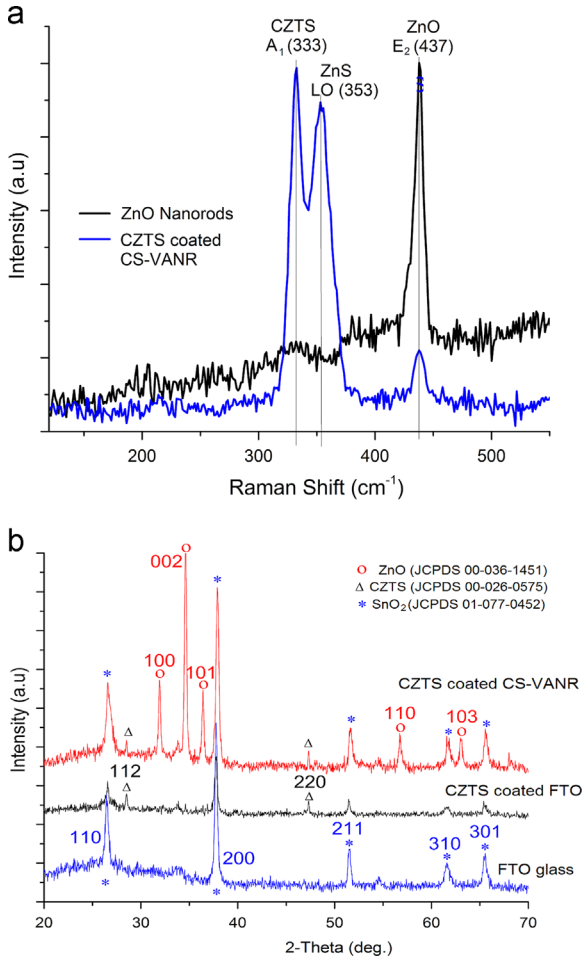

Fig. 5. (a) Raman spectra of the ZnO nanorods and CZTS coated ZnO/ZnS core/shell nanorods and (b) XRD patterns of the substrate surface (FTO-coated glass), spin coated and annealed film of CZTS nanoparticles over substrate and CZTS-coated ZnO/ZnS CS-VANR over substrate.

nanoparticles size is ideal for the device fabrication since it will not only enable uniform surface coverage of the CS-VANRs, but also lead to mesoporous structure formation with fine pore size. HRTEM image of CZTS nanocrystal is given in Fig. 3(d), (112) planes are clearly visible and have been marked for lattice fringe distance of 0.31 nm. The SEM microstructure of the post-annealed CZTS coated CS-VANR shown in Fig. 4c where the vertically aligned array is completely covered by the CZTS nanoparticles at the top along with porous structure with pore size of the order of few tens of nanometers. The mesoporous structure is formed presumably due to inefficient packing of the CZTS nanoparticles, ethanol evaporation during annealing as well as thermal decomposition of any volatile organic species remaining from nanoparticles synthesis step and is beneficial from the point of view of liquid electrolyte uptake during fabrication of liquid junction solar cells.

The ZnS formation was also confirmed by performing Raman spectroscopy of the samples after ion exchange treatment, as presented in Fig. 5a. The lines to indicate peak position are drawn as a guide to the eye. The E_{2h} peak positioned at 437 cm^{-1} is due to nonpolar Raman active mode and is characteristic of bare ZnO nanorods. Upon CZTS nanoparticles' deposition over ZnO/ZnS core/shell nanostructures, additional peaks appear at 333 and 353 cm^{-1} whereas intensity of the peak at 437 cm^{-1} is reduced. The peak at 333 cm^{-1} is attributed to A_1 symmetry of kesterite CZTS which is purely anion mode and is due to vibration of S atoms surrounded by motionless neighboring atoms [43,44]. The

presence of the other peak (at 353 cm^{-1}) is due to strong first-order longitudinal optical (LO) scattering mode of the cubic ZnS [45,46]. The findings corroborate the observations made during HRTEM examination of the samples.

Fig. 5b shows the XRD patterns of the FTO-coated conducting substrate, CZTS film produced over the substrate and CZTS nanoparticles deposited over CS-VANR array. The SnO_2 film over the glass sheet appears as peaks representing tetragonal SnO_2 phase (JCPDS 01-077-0452) [47]. The XRD analysis of the CZTS-coated substrate indicates a tetragonal crystal structure (JCPDS 00-026-0575) with two peaks representative of (112) and (220) planes of the kesterite phase [48]. The CZTS-coated ZnO/ZnS or ZnO/ZnSe core/shell nanostructures shows peaks that can be indexed to be from hexagonal ZnO (JCPDS 00-036-1451) [39] only with preferred orientation along (002) plane or growth in [001] direction while peaks of CZTS and FTO are also present. Although peaks characteristic of ZnS or ZnSe phase are not visible in the XRD pattern perhaps due to their extremely small thicknesses, the evidence for their presence is nevertheless available from HRTEM examination.

Photovoltaic performance of the fabricated liquid junction solar cells having a surface area of 0.2 cm^2 was evaluated under 1 Sun illumination (100 mW/cm^2) and the output current density–voltage (J–V) data is graphically shown in Fig. 6. The solar cell based on CS-VANR-1 demonstrates a short-circuit current density (J_{SC}), open circuit voltage (V_{OC}) and fill factor values of 4.65 mA/cm^2, 470 mV and 0.4, respectively, which correspond to the power conversion efficiency (η) of 0.85%. This lower efficiency is mainly because of high conduction band offset between ZnS and CZTS. CS-VANR-2 employing ZnSe as buffer layer exhibits improved J_{SC}, V_{OC} and fill factor values of 10.46 mA/cm2, 0.49 V and 0.43, respectively, which correspond to the power conversion efficiency (η) of 2.2%. To investigate the peculiar role of 1-D nanostructures towards photovoltaic conversion enhancement and for comparison with their thin films based counterparts, planer ZnO/ZnS thin films configuration sensitized with CZTS nanoparticles was fabricated using ZnO film on FTO as initial structure through surface ZnO phase conversion to ZnS and subsequent CZTS nanoparticles coating and liquid junction solar cell fabrication using the same procedure as that adopted for 1-D structures. The planar ZnO/ZnS-CZTS solar cell device yielded a PCE of 0.12% with associated J_{SC} of 0.6 mA/cm^2 and Voc of 0.5 V, as shown in Fig. 6.

Solar cell characteristics of all three cells are given in Table 1, which provides insight of devices. V_{OC} and J_{SC} values are directly obtained from JV curve intercepts on the x-axis and y-axis respectively while fill factor (FF) was calculated from ratio of

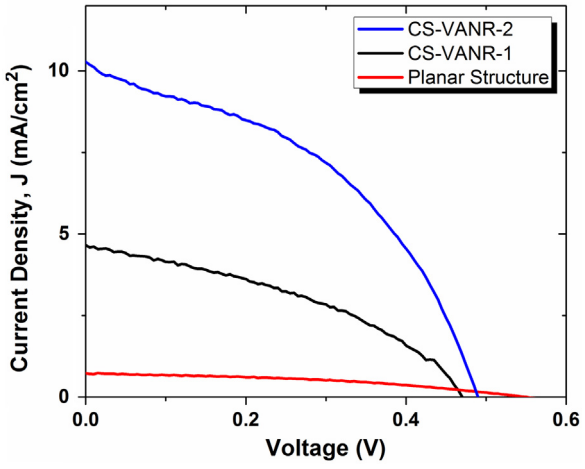

Fig. 6. Comparison of current density–voltage (J–V) data for CZTS sensitized ZnO based liquid junction solar cells with CS-VANRs configurations and planar heterostructure.

actual maximum power output to theoretical power. While shunt resistance was calculated from smoothed $J-V$ curve by plotting dV/dJ against V near J_{SC}, series resistance (R_S) was calculated by plotting dV/dJ against $(J+J_{SC}-GV)^{-1}$ and using diode equation, where G is the shunt conductance [49]. Here, it is clear that although the planar device has reasonable shunt resistance of 1783.7 Ω cm^2, the series resistance value of 83.3 Ω cm^2 is also high enough to reduce the J_{SC} primarily due to longer charge transport distances involving large number of grain boundaries before they are taken-up by counter electrode. This series resistance is reduced greatly by involving 1-D core/shell nanostructures as charge transfer distances are smaller owing to less number of grain boundaries in flow of charge carriers. But shunt resistance (R_{SH}) decreases because of larger interfacial area, chances of shunt paths increases thereby reducing the V_{OC} compared with planar structure.

The superior cell performance seen in case of core/shell vertically-aligned nanorods array structure may be attributed to efficient light absorption and improved charge transport in 1-D nanostructures as evident from external quantum efficiency (EQE) plots in Fig. 7. The incident photon conversion efficiency (IPCE) or external quantum efficiency (EQE) values for planar structure are very low which is obvious as the film thickness is very low to make materials quantity comparable with 1-D nanostructure based devices. In case of CS-VANR-1 device i.e. 1-D nanostructured cell based on ZnS buffer layer, the spread of plot is near to ideal square shape with very high IPCE values. On the other hand, the CS-VANR-2 solar cell incorporating ZnSe buffer layer yields even higher IPCE values since the conduction band offset is lower between ZnSe and CZTS compared with ZnS and CZTS, thus resulting in improved charge transport and better EQE. Band gaps can be calculated for all three cells from their EQE plots by plotting the $[h\nu_x \ln(1-EQE)]^2$ vs photon energy (eV) as shown in Fig. 7, almost all compositions have similar band gap of 1.5 eV as all of them have same CZTS nanocrystals as absorber layer. The nanocrystalline nature of CZTS enables effective light harvesting via scattering from very large grain boundary area in the direction of light propagation owing to nanoscale size of the CZTS particles. For charge transport, the electrons will need to migrate from CZTS nanocrystals to the Al:ZnO nanorods at the core through thin buffer shell. The transport distance for charge carriers, therefore, is very small before these can be accommodated by the respective electrodes, thus drastically reducing any chances of carrier recombination. Thus, efficient light harvesting combined with improved charge separation and transport due to nanoparticles-coated vertically aligned nanorods architecture reflect in the form of improved short-circuit current density (J_{SC}) values and enhanced power conversion efficiency.

A comparison of the cell area for one-dimensional core/shell superstrate device configuration employed in this work with thin film planar configuration, for the same set of material compositions reveals an increase in the interfacial area by a factor of ~8.7. In other words, for 1 μm^2 cell area, the CS-VANR-1 made up of nanorods with 75 nm diameter and 100 nm inter-nanorod spacing and subsequently sensitized with CZTS nanoparticles, offers an interfacial area of 8.7 μm^2 for a Cd-free superstrate solar cell architecture. The estimated 8.7 times increase in the interfacial area is anticipated to cause approximately 7-fold increase in the solar cell efficiency besides enhancement in optoelectronic properties.

Lee et al. have recently reported CS VANR arrays based solar cells comprising of Au/CZTS-NP/CdS/ZnO NR/ITO [26]. Here the planar counter electrode is in contact with the CZTS particles which completely fill the spaces between and over the nanorods. So, the charge carriers have to pass a large number of nanocrystals/boundaries to reach the collecting electrode resulting in a

Table 1
Device characteristics of solar cells calculated from *J–V* plots.

	Composition	J_{SC} (mA/cm^2)	V_{OC} (V)	FF	R_S (ohm cm^2)	R_{SH} (ohm cm^2)	Efficiency (%)
Planar structure	FTO/ZnO/Al:ZnO/ZnS/CZTS	0.73	0.55	0.4	83.33	1783.7	0.16
CS-VANR-1	FTO/ZnO/Al:ZnO/ZnS/CZTS	4.65	0.47	0.4	10.20	227.7	0.85
CS-VANR-2	FTO/ZnO/Al:ZnO/ZnSe/CZTS	10.46	0.49	0.43	14.01	64.8	2.2

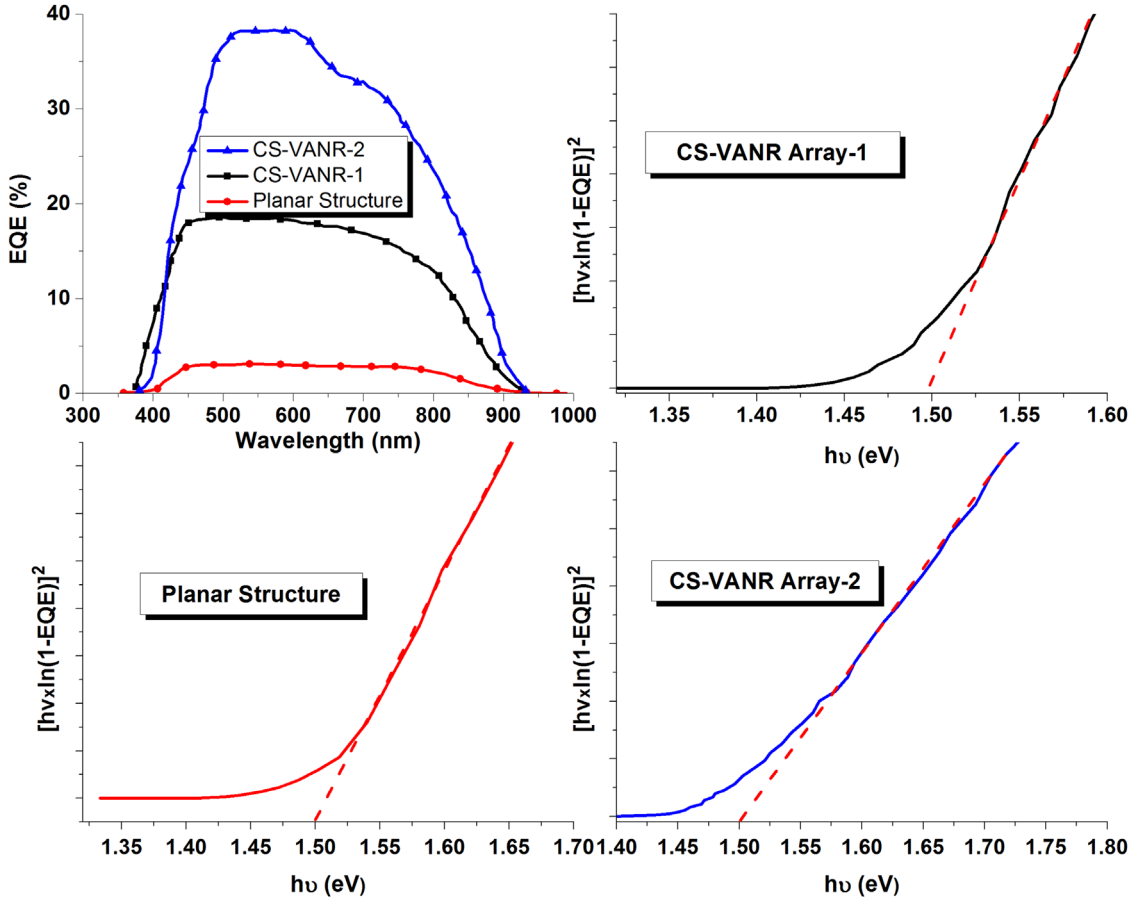

Fig. 7. External quantum efficiency plots of Planar and 1-D nanostructured solar cell and band gap calculations from EQE data.

lower J_{SC} value. Similarly Jiang et al. reported a Au/Spiro-MeOTAD/CZTS-NP/CdS/ZnO-NR/ZnO/FTO configuration [27] with improved interface between the counter electrode and the absorber layer through incorporation of a hole transport material i.e. spiro OMeTAD resulting in higher J_{SC} values. However, the absorber/electrolyte/counter electrode interfaces were smooth leaving room for improvement by increasing the interface area. We have increased the interfacial area between absorber/electrolyte by adding mesoporous architecture allowing infusion of the electrolyte into the absorber layer to extract more charge carriers and transporting them to the collecting electrodes. Thus, the electrolyte can penetrate into the porous structure and extract charge carriers near the generation point, which also decreases the chances of recombination and series resistance value due to shorter travel distances and involvement of less number of grain boundaries.

Although the reported efficiency values in current work and related reports [26,27] based on similar nanostructures are small compared with other well-established thin film configurations [13], careful optimization of the nanorods array attributes including diameter, length, aspect ratio and inter-nanorods spacing have strong potential to greatly improve cell performance for technology scale-up and commercialization.

4. Conclusions

A unique solar cell configuration based on core–shell vertically aligned nanorods assembly involving solution processing routes is proposed and presented. A superstrate liquid junction solar cell device is fabricated over FTO coated glass via sequential growth of vertically aligned Al:ZnO nanorods over ZnO blocking layer, a thin ZnS or ZnSe layer formation through ion exchange, CZTS nanoparticles deposition and subsequent joining with the Cu_2S counter-electrode with inter-electrode space filled with polysulfide electrolyte. The ZnS or ZnSe buffer layer formation occurs by anion exchange method in S^{2-} or Se^{2-} solution at low temperature to spontaneously convert ZnO nanorods surface to respective buffer chalcogenide due to differences in K_{sp} values. The *J–V* measurements of such solar cell (FTO/ZnO/Al:ZnO/ZnSe/CZTS) demonstrated a conversion efficiency of 2.2% with respective values of J_{SC}, V_{OC} and FF to be 10.46 mA/cm^2, 0.49 V and 0.43, respectively. The cell performance is superior to its thin film based

counterpart, presumably due to a multifold increase in the interfacial area, greater degree of light harvesting and efficient charge transport. The nanorod's length, aspect ratio and inter-rods spacing needs to be optimized for further enhancement in solar cell performance.

Acknowledgments

This work was supported by the Higher Education Commission of Pakistan (NRPU Grant # 1603).

The authors gratefully acknowledge the technical and financial support of the Research Center of College of Engineering, Deanship of Scientific Research, King Saud University, Saudi Arabia.

References

[1] A. Chirila, P. Reinhard, F. Pianezzi, P. Bloesch, A.R. Uhl, C. Fella, L. Kranz, D. Keller, C. Gretener, H. Hagendorfer, D. Jaeger, R. Erni, S. Nishiwaki, S. Buecheler, A.N. Tiwari, Potassium-induced surface modification of Cu(In,Ga)Se_2 thin films for high-efficiency solar cells, Nat. Mater. 12 (2013) 1107–1111.

[2] M. Gloeckler, I. Sankin, Z. Zhao, CdTe solar cells at the threshold to 20% efficiency, IEEE J. Photovolt. 3 (2013) 1389–1393.

[3] M.A. Green, K. Emery, Y. Hishikawa, W. Warta, E.D. Dunlop, Solar cell efficiency tables (version 43), Prog. Photovolt.: Res. Appl. 22 (2014) 1–9.

[4] B.A. Andersson, Materials availability for large-scale thin-film photovoltaics, Prog. Photovolt.: Res. Appl. 8 (2000) 61–76.

[5] D.B. Mitzi, O. Gunawan, T.K. Todorov, K. Wang, S. Guha, The path towards a high-performance solution-processed kesterite solar cell, Sol. Energy Mater. Sol. Cells 95 (2011) 1421–1436.

[6] M. Kakei, T. Sakae, M. Yoshikawa, Combined effects of estrogen deficiency and cadmium exposure on calcified hard tissues: animal model relating to itai–itai disease in postmenopausal women, Proc. Jpn. Acad. Ser. B Phys. Biol. Sci. 89 (2013) 340–347.

[7] Z. Fang, X.C. Wang, H.C. Wu, C.Z. Zhao, Achievements and challenges of CdS/CdTe solar cells, Int. J. Photoenergy 2011 (2011) 1–8.

[8] A. Khalkar, K.-S. Lim, S.-M. Yu, S.P. Patole, J.-B. Yoo, Effect of growth parameters and annealing atmosphere on the properties of Cu_2ZnSnS_4 thin films deposited by cosputtering, Int. J. Photoenergy 2013 (2013) 1–7.

[9] X. Lin, J. Kavalakkatt, K. Kornhuber, S. Levcenko, M.C. Lux-Steiner, A. Ennaoui, Structural and optical properties of Cu_2ZnSnS_4 thin film absorbers from ZnS and Cu_3SnS_4 nanoparticle precursors, Thin Solid Films 535 (2013) 10–13.

[10] C. Steinhagen, M.G. Panthani, V. Akhavan, B. Goodfellow, B. Koo, B.A. Korgel, Synthesis of Cu(2)ZnSnS(4) nanocrystals for use in low-cost photovoltaics, J. Am. Chem. Soc. 131 (2009) 12554–12555.

[11] K. Tanaka, M. Oonuki, N. Moritake, H. Uchiki, $Cu_2ZnSnS_4Cu_2ZnSnS_4$ thin film solar cells prepared by non-vacuum processing, Sol. Energy Mater. Sol. Cells 93 (2009) 583–587.

[12] B. Shin, O. Gunawan, Y. Zhu, N.A. Bojarczuk, S.J. Chey, S. Guha, Thin film solar cell with 8.4% power conversion efficiency using an earth-abundant Cu_2ZnSnS_4 absorber, Prog. Photovolt.: Res. Appl. 21 (2013) 72–76.

[13] W. Wang, M.T. Winkler, O. Gunawan, T. Gokmen, T.K. Todorov, Y. Zhu, D. B. Mitzi, Device characteristics of CZTSSe thin-film solar cells with 12.6% efficiency, Adv. Energy Mater. 4 (2014).

[14] K. Ramanathan, M.A. Contreras, C.L. Perkins, S. Asher, F.S. Hasoon, J. Keane, D. Young, M. Romero, W. Metzger, R. Noufi, J. Ward, A. Duda, Properties of 19.2% efficiency ZnO/CdS/CuInGaSe_2 thin-film solar cells, Prog. Photovolt.: Res. Appl. 11 (2003) 225–230.

[15] I. Repins, M.A. Contreras, B. Egaas, C. DeHart, J. Scharf, C.L. Perkins, B. To, R. Noufi, 19.9%—efficient ZnO/CdS/CuInGaSe_2 solar cell with 81.2% fill factor, Prog. Photovolt.: Res. Appl. 16 (2008) 235–239.

[16] J.S. Ward, K. Ramanathan, F.S. Hasoon, T.J. Coutts, J. Keane, M.A. Contreras, T. Moriarty, R. Noufi, A 21.5% efficient Cu(In,Ga)Se_2 thin-film concentrator solar cell, Prog. Photovolt.: Res. Appl. 10 (2002) 41–46.

[17] T. Kameyama, T. Osaki, K.-i Okazaki, T. Shibayama, A. Kudo, S. Kuwabata, T. Torimoto, Preparation and photoelectrochemical properties of densely immobilized Cu_2ZnSnS_4 nanoparticle films, J. Mater. Chem. 20 (2010) 5319.

[18] Y. Kim, K. Woo, I. Kim, Y.S. Cho, S. Jeong, J. Moon, Highly concentrated synthesis of copper–zinc–tin–sulfide nanocrystals with easily decomposable capping molecules for printed photovoltaic applications, Nanoscale 5 (2013) 10183–10188.

[19] H.-C. Liao, M.-H. Jao, J.-J. Shyue, Y.-F. Chen, W.-F. Su, Facile synthesis of wurtzite copper–zinc–tin sulfide nanocrystals from plasmonic djurleite nuclei, J. Mater. Chem. A 1 (2013) 337.

[20] W.C. Liu, B.L. Guo, X.S. Wu, F.M. Zhang, C.L. Mak, K.H. Wong, Facile hydrothermal synthesis of hydrotropic Cu_2ZnSnS_4 nanocrystal quantum dots: band-gap engineering and phonon confinement effect, J. Mater. Chem. A 1 (2013) 3182.

[21] S.W. Shin, J.H. Han, Y.C. Park, G.L. Agawane, C.H. Jeong, J.H. Yun, A.V. Moholkar, J.Y. Lee, J.H. Kim, A facile and low-cost synthesis of promising absorber materials on $Cu_2ZnSn(S_xSe_{1-x})_4$ nanocrystals consisting of earth abundant elements with tunable band gap characteristics, J. Mater. Chem. 22 (2012) 21727.

[22] K. Yu, J. Chen, Enhancing solar cell efficiencies through 1-D nanostructures, Nanoscale Res. Lett. 4 (2008) 1–10.

[23] M. Yu, Y.Z. Long, B. Sun, Z. Fan, Recent advances in solar cells based on one-dimensional nanostructure arrays, Nanoscale 4 (2012) 2783–2796.

[24] M.A. Akram, S. Javed, J. Xu, M. Mujahid, C.-S. Lee, Arrays of ZnO/$CuIn_xGa_{1-x}Se_2$ nanocables with tunable shell composition for efficient photovoltaics, J. Appl. Phys. 117 (2015) 205306.

[25] J. Xu, C.Y. Luan, Y.B. Tang, X. Chen, J.A. Zapien, W.J. Zhang, H.L. Kwong, X. M. Meng, S.T. Lee, C.S. Lee, Low-temperature synthesis of $CuInSe_2$ nanotube array on conducting glass substrates for solar cell application, ACS Nano 4 (2010) 6064–6070.

[26] L. Dongwook, Y. Kijung, Solution-processed Cu_2ZnSnS_4 superstrate solar cell using vertically aligned ZnO nanorods, Nanotechnology 25 (2014) 065401.

[27] M. Jiang, J. Wu, G. Di, G. Li, Nanostructured solar cell based on solution processed Cu_2ZnSnS_4nanoparticles and vertically aligned ZnO nanorod array, Phys. Status Solidi (RRL)-Rapid Res. Lett. 8 (2014) 971–975.

[28] A. Yamada, K. Matsubara, K. Sakurai, S. Ishizuka, H. Tampo, P.J. Fons, K. Iwata, S. Niki, Effect of band offset on the open circuit voltage of heterojunction $CuIn_{[1-x]}Ga_{[x]}Se_{[2]}$ solar cells, Appl. Phys. Lett. 85 (2004) 5607.

[29] M. Addou, A. Moumin, Ei B, M. Regragui, A. Bougrine, A. Kachouane, C. Monty, Structural, optical and electrical properties of undoped and indium doped zinc oxide prepared by spray pyrolysis, J. Chim. Phys. 96 (1999) 232–244.

[30] T. Nakada, M. Mizutani, Improved efficiency of Cu(In,Ga)Se_2 thin film solar cells with chemically deposited ZnS buffer layers by air-annealing-formation of homojunction by solid phase diffusion, in: Proceedings of the Twenty-Eighth IEEE Photovoltaic Specialists Conference, Conference Record, 2000, pp. 529–534.

[31] M.A. Contreras, T. Nakada, M. Hongo, A.O. Pudov, J.R. Sites, ZnO/ZnS(O,OH)/Cu(In,Ga)Se_2/Mo solar cell with 18.6% efficiency, in: Proceedings of the 3rd World Conference on Photovoltaic Energy Conversion, vol. 571, 2003, pp. 570–573.

[32] K. Kushiya, Development of Cu(InGa)Se_2-based thin-film PV modules with a $Zn(O,S,OH)_x$ buffer layer, Sol. Energy 77 (2004) 717–724.

[33] A. Nagoya, R. Asahi, G. Kresse, First-principles study of Cu_2ZnSnS_4 and the related band offsets for photovoltaic applications, J. Phys. Condens. Matter: Inst. Phys. J. 23 (2011) 404203.

[34] D.A.R. Barkhouse, R. Haight, N. Sakai, H. Hiroi, H. Sugimoto, D.B. Mitzi, Cd-free buffer layer materials on $Cu_2ZnSn(S_xSe_{1-x})4$: Band alignments with ZnO, ZnS, and In2S3, Appl. Phys. Lett. 100 (2012) 193904.

[35] A. Santoni, F. Biccari, C. Malerba, M. Valentini, R. Chierchia, A. Mittiga, Valence band offset at the CdS/Cu_2ZnSnS_4 interface probed by x-ray photoelectron spectroscopy, J. Phys. D.: Appl. Phys. 46 (2013) 175101.

[36] H. Hagendorfer, K. Lienau, S. Nishiwaki, C.M. Fella, L. Kranz, A.R. Uhl, D. Jaeger, L. Luo, C. Gretener, S. Buecheler, Y.E. Romanyuk, A.N. Tiwari, Highly transparent and conductive ZnO:Al thin films from a low temperature aqueous solution approach, Adv. Mater. 26 (2014) 632–636.

[37] E. Edri, E. Rabinovich, O. Niitsoo, H. Cohen, T. Bendikov, G. Hodes, Uniform coating of light-absorbing semiconductors by chemical bath deposition on sulfide-treated ZnO Nanorods, J. Phys. Chem. C. 114 (2010) 13092–13097.

[38] V. Gonzalez-Pedro, X. Xu, I. Mora-Sero, J. Bisquert, Modeling high-efficiency quantum dot sensitized solar cells, ACS Nano 4 (2010) 5783–5790.

[39] S. Salam, M. Islam, A. Akram, Sol–gel synthesis of intrinsic and aluminum-doped zinc oxide thin films as transparent conducting oxides for thin film solar cells, Thin Solid Films 529 (2013) 242–247.

[40] S. Xu, N. Adiga, S. Ba, T. Dasgupta, C.F. Wu, Z.L. Wang, Optimizing and improving the growth quality of ZnO nanowire arrays guided by statistical design of experiments, ACS Nano 3 (2009) 1803–1812.

[41] S. Xu, C. Lao, B. Weintraub, Z.L. Wang, Density-controlled growth of aligned ZnO nanowire arrays by seedless chemical approach on smooth surfaces, J. Mater. Res. 23 (2011) 2072–2077.

[42] J.R. Goates, M.B. Gordon, N.D. Faux, Calculated values for the solubility product constants of the metallic sulfides, J. Am. Chem. Soc. 74 (1952) 835–836.

[43] W. Li, K. Jiang, J. Zhang, X. Chen, Z. Hu, S. Chen, L. Sun, J. Chu, Temperature dependence of phonon modes, dielectric functions, and interband electronic transitions in Cu_2ZnSnS_4 semiconductor films, Phys. Chem. Chem. Phys.: PCCP 14 (2012) 9936–9941.

[44] M. Grossberg, J. Krustok, J. Raudoja, K. Timmo, M. Altosaar, T. Raadik, Photoluminescence and Raman study of $Cu_2ZnSn(Se_xS_{1-x})4$ monograins for photovoltaic applications, Thin Solid Films 519 (2011) 7403–7406.

[45] J.H. Kim, H. Rho, J. Kim, Y.J. Choi, J.G. Park, Raman spectroscopy of ZnS nanostructures, J. Raman Spectrosc. 43 (2012) 906–910.

[46] W. Nilsen, Raman Spectrum of Cubic ZnS, Phys. Rev. 182 (1969) 838–850.

[47] R. Riveros, E. Romero, G. Gordillo, Synthesis and characterization of highly transparent and conductive SnO_2:F and In_2O_3:Sn thin films deposited by spray pyrolysis, Braz. J. Phys. 36 (2006) 1042–1045.

[48] J. Zhang, B. Long, S. Cheng, W. Zhang, Effects of sulfurization temperature on properties of CZTS films by vacuum evaporation and sulfurization method, Int. J. Photoenergy 2013 (2013) 1–6.

[49] H. Chen, Q. Ye, X. He, J. Ding, Y. Zhang, J. Han, J. Liu, C. Liao, J. Mei, W. Lau, Electrodeposited CZTS solar cells from Reline electrolyte, Green Chem. 16 (2014) 3841–3845.